SUPPLEMENTAL INFORMATION

Experimental Configuration

Figure S1 shows schematics of the reaction setups used for the in situ experiments. Figure S1a shows the configuration used to monitor reactions in aqueous solution in experiments (b) and (c). The configuration shown in S1b was used to monitor reactions at the air-ice interface in (b), (d), and (e), as well as at the air-water interface in (e). The configuration in S1c was used to monitor reactions at the air-ice and air-water interface in (e).

Actinometry

Hydrogen peroxide, nitrite, and nitrate undergo photolysis in aqueous solution to form hydroxyl radicals (see for example (Chu and Anastasio 2003; 2005; 2007) and references therein):

$$H_2O_2 \xrightarrow{\;h\nu\;} 2OH \qquad \textbf{(R2)}$$

$$NO_2^- \xrightarrow{\;h\nu,H^+\;} NO + OH \qquad \textbf{(R3)}$$

$$NO_3^- \xrightarrow{\;h\nu\;} NO_2^- + O$$

(R1)

Benzene and OH react to form phenol with a yield of 0.95 (Vione et al. 2006). We therefore used benzene as a hydroxyl radical trap and monitored phenol production. For this technique, the following reactions are important:

$$Ox + h\nu \xrightarrow{\;J_{OH}\;} OH \qquad \textbf{(R4)}$$

$$OH + B \xrightarrow{\;k_B\;} P \qquad \textbf{(R5)}$$

$$OH + Ph \xrightarrow{\;k_P\;} P \qquad \textbf{(R6)}$$

where Ox is either H_2O_2, NO_2^-, or NO_3^-, J_{OH} is the photolysis rate constant for OH formation, B is benzene, k_B is the second order rate constant for the reaction between benzene and OH, P is products, Ph is phenol, and k_P is the second order rate constant for the reaction between phenol and OH. Since we only used data from short irradiation times, when phenol concentrations were very low, R6 was negligible under our

experimental conditions and could be ignored. Reaction 5 forms phenol with a 95% yield (Vione et al. 2006), which leads us to the following expression:

$$OH + B \xrightarrow{0.95k_B} Ph \tag{R7}$$

Since k_B is large and the initial benzene concentrations were always equal to or greater than initial oxidant concentrations, we expect that $k_B[OH][B]$ was greater than $J_{Ox}[Ox]$, and so the steady-state assumption was valid for [OH] under our experimental conditions:

$$\frac{d[OH]}{dt} = J_{OH}[Ox] - k_B[OH][B] \approx 0 \tag{8}$$

Rearranging Eq. 8 gives us an expression for the steady-state concentration of OH:

$$[OH]_{ss} = \frac{J_{OH}[Ox]}{k_B[B]} \tag{9}$$

The parameter measured in these experiments was $\dfrac{d[Ph]}{dt}$. Phenol concentrations were determined from the measured fluorescence intensity using a calibration curve (Fig. S2). Equation 10 gives the rate expression for phenol formation in our experiments:

$$\frac{d[Ph]}{dt} = 0.95k_B[OH][B] \tag{10}$$

Substituting Eq. 9 into Eq. 10 and rearranging the expression gives us J_{OH}:

$$J_{OH} = \frac{d[Ph]}{dt}\left(0.95[Ox]\right)^{-1} \tag{11}$$

We determined J_{OH} by plotting the phenol growth rate as a function of oxidant concentration, as illustrated in Figure 6 in the manuscript. The slopes of the linear fits to the data give $0.95(J_{OH})$. The photolysis rate constants determined in this manner for nitrite, hydrogen peroxide, and nitrate are respectively 8.64×10^{-6} s^{-1}, 3.67×10^{-7} s^{-1}, and 2.41×10^{-7} s^{-1}. It should be noted that at concentrations above $\sim 4 \times 10^{-5}$ mol L^{-1} NO$_2^-$, phenol's growth rate levels off, as illustrated in Figure S3. This does not affect our calculations of J_{OH}, as we used NO$_2^-$ concentrations below this level. It could, however, explain low nitrite photolysis rate constants (Galbavy et al. 2007) measured at high nitrite

concentrations. This behaviour should be kept in mind for future experiments using nitrite as an actinometer.

We determined $[OH]_{ss}$ by measuring phenol's formation rate as a function of benzene concentration, at a constant nitrite concentration of 2.95×10^{-5} mol L^{-1}. The slope of the linear fit to the data in Figure S4 yields $k_B[OH]_{ss}$. The intercept in Figure S4 is zero within the error of the measurements. This suggests that reaction with benzene to form phenol is the major loss process for OH. If other processes were important, we would expect non-linear behaviour at low benzene concentrations, as reaction with benzene would be in competition with some other loss process; it is clear from our data that this is not the case. Dividing the slope by k_B (= 7.8×10^9 L mol^{-1} s^{-1}) (Buxton et al. 1988) gives $[OH]_{ss} = 2.15 \times 10^{-18}$ mol L^{-1}. This concentration is very low, as expected under steady-state conditions.

As a final test of our technique, we used our measured J_{OH} for each oxidant to calculate photon fluxes for our lamp using the following equation:

$$J_{OH} = \int_{\lambda_\circ}^{\lambda} \sigma(\lambda)\Phi(\lambda)F_\lambda \, d\lambda \tag{12}$$

Where $\sigma(\lambda)$ is the absorption cross section of the oxidant at a given wavelength, $\Phi(\lambda)$ is the quantum yield of OH formation, and F_λ is the photon flux. Using absorption cross sections and photolysis quantum yields from the literature (Chu and Anastasio 2003; 2005; 2007), we calculated photon fluxes across the wavelength range of absorption of each oxidant. The results are summarized in Table S1.

Dividing the total photon flux by the wavelength range yields the average photon flux at each wavelength. The average fluxes predicted by the three OH precursors agree within a factor of three. The photon flux of the lamp predicted by the manufacturer is 1.41×10^{12} photons cm^{-2} s^{-1} nm^{-1} in the wavelength range of interest in this study. Our calculated average photon fluxes agree with that prediction within a factor of ten.

HPLC Methodology

Melted samples from the experiments described in Section 3.1.1 of the manuscript were analyzed for the presence of phenol using a Waters HPLC-UV with a diode array detector. The column was a C18 (Jones Chromatography, 25 cm x 4.6 mm x 4 μm). A 90:10 acetonitrile-water mixture was run isocratically at a flow rate of 1 mL min^{-1}. Absorption was monitored at 210 nm. Phenol eluted at 3.6 min, and benzene eluted at 5 min.

References

Buxton, G. V., C. L. Greenstock, W. P. Helman and A. B. Ross: Critical-Review of Rate Constants for Reactions of Hydrated Electrons, Hydrogen-Atoms and Hydroxyl Radicals (.Oh/.O-) in Aqueous-Solution. Journal of Physical and Chemical Reference Data, 17, 513-886, 1988.

Chu, L. and C. Anastasio: Quantum yields of hydroxyl radical and nitrogen dioxide from the photolysis of nitrate on ice. J. Phys. Chem., 107, 9594-9602, 2003.

Chu, L. and C. Anastasio: Formation of hydroxyl radical from the photolysis of frozen hydrogen peroxide. Journal of Physical Chemistry A, 109, 6264-6271, 2005.

Chu, L. and C. Anastasio: Temperature and wavelength dependence of nitrite photolysis in frozen and aqueous solutions. Environmental Science & Technology, 41, 3626-3632, 2007.

Galbavy, E. S., C. Anastasio, B. L. Lefer and S. R. Hall: Light penetration in the snowpack at Summit, Greenland: Part I - Nitrite and hydrogen peroxide photolysis. Atmospheric Environment, 41, 5077-5090, 2007.

Vione, D., G. Falletti, V. Maurino, C. Minero, E. Pelizzetti, M. Malandrino, R. Ajassa, R. I. Olariu and C. Arsene: Sources and sinks of hydroxyl radicals upon irradiation of natural water samples. Environmental Science & Technology, 40, 3775-3781, 2006.

Table S1. Calculated photon fluxes based on measured J_{OH}

Oxidant	Wavelengths (nm)	Total Flux (photon cm^{-2} s^{-1})	Average Flux (photon cm^{-2} s^{-1} nm^{-1})
NO_2^-	295 – 410	4.45×10^{13}	3.87×10^{11}
H_2O_2	295 – 330	4.99×10^{12}	1.43×10^{11}
NO_3^-	296 – 360	1.37×10^{13}	2.14×10^{11}

Figure S1. Schematic of the experimental configuration used to monitor reactions (a) in aqueous solution; (b) at air-ice and air-water interfaces with the lamp's output hitting the sample from above; and (c) at air-ice and air-water interfaces with the lamp's output entering the chamber horizontally and illuminating the region directly above the sample.

Figure S2. Beer-Lambert plots for phenol in aqueous solution for offline and in situ measurements. The traces are linear fits to the data. Error bars represent one standard deviation about the mean of at least three trials.

Figure S3. Dependence of phenol formation rate on nitrite concentration in solution in the presence of 1.2×10^{-3} mol L^{-1} benzene. Error bars represent one standard deviation about the mean of at least two trials.

Figure S4. Dependence of phenol formation rate on benzene concentration in the presence of 2.95×10^{-5} mol L^{-1} nitrite. The solid trace is a linear fit to the data. Error bars represent one standard deviation about the mean of at least two trials.
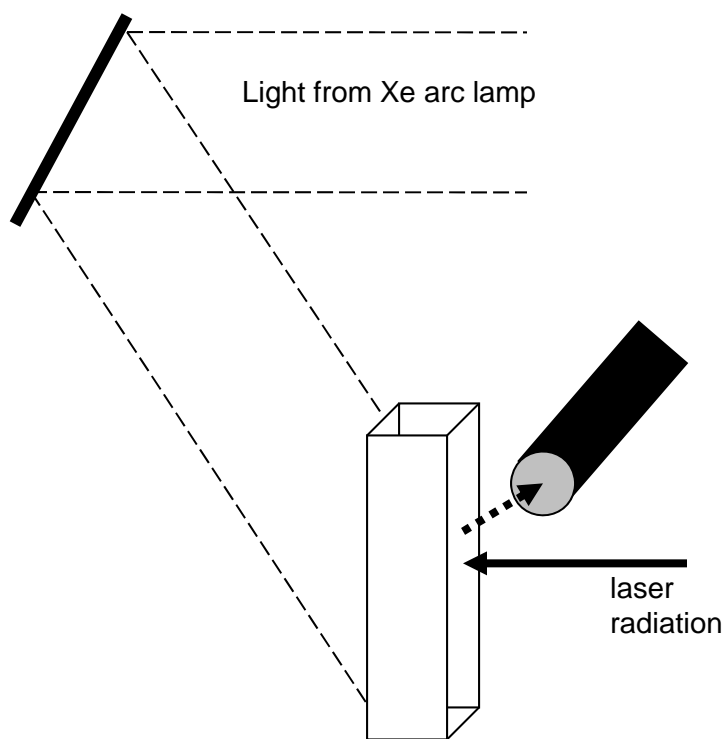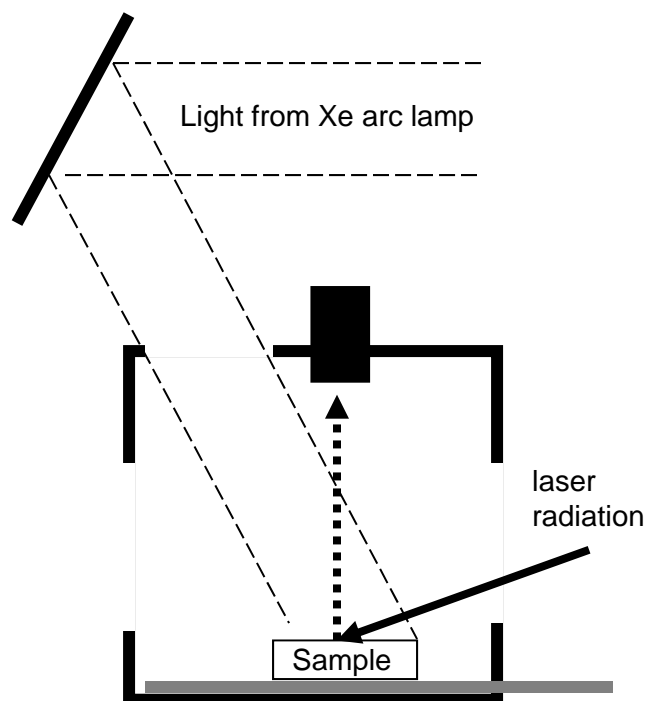
Light from Xe arc lamp

laser
radiation

Figure S1a

Light from Xe arc lamp

laser
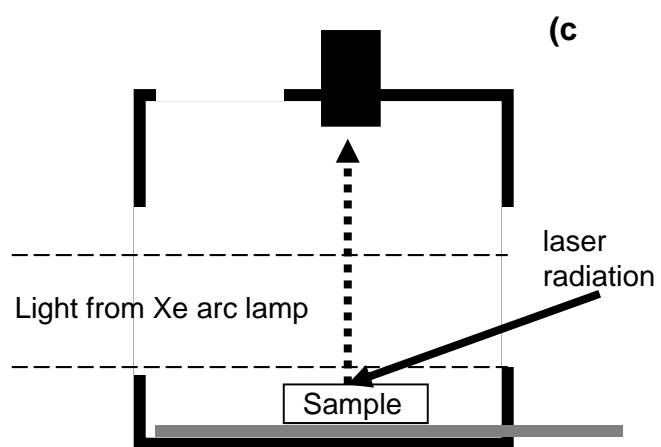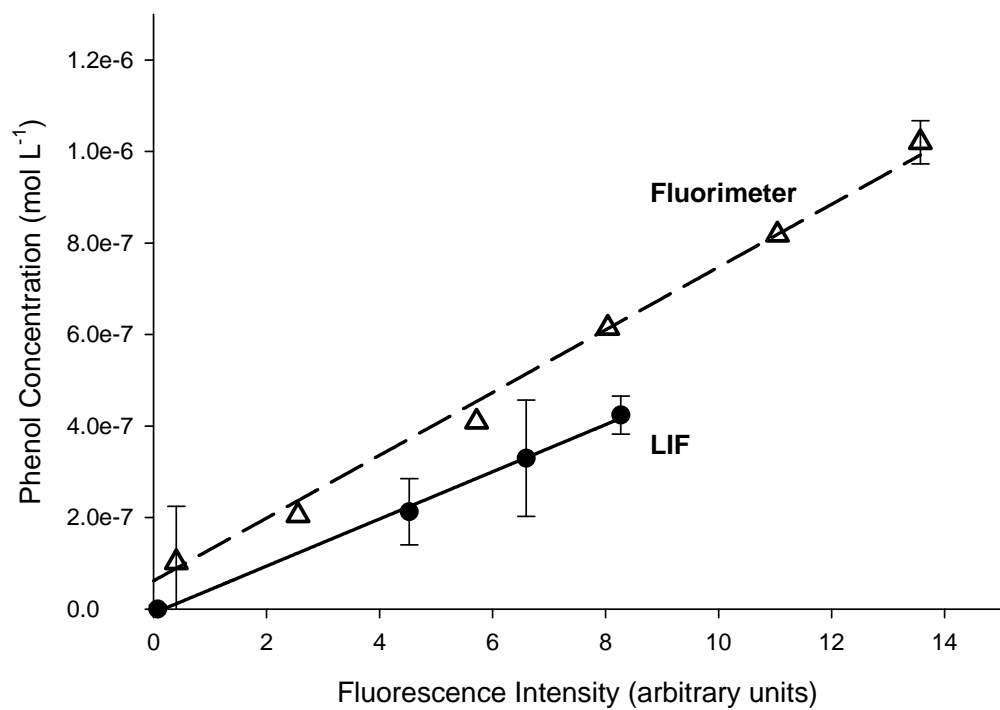radiation

Sample

Figure S1b

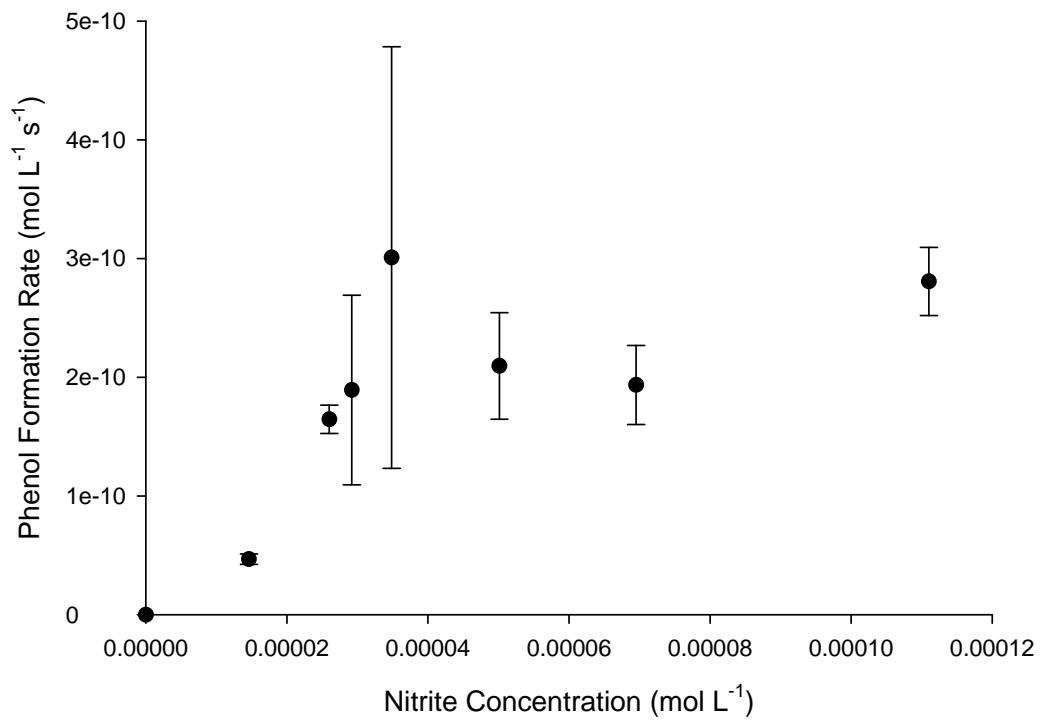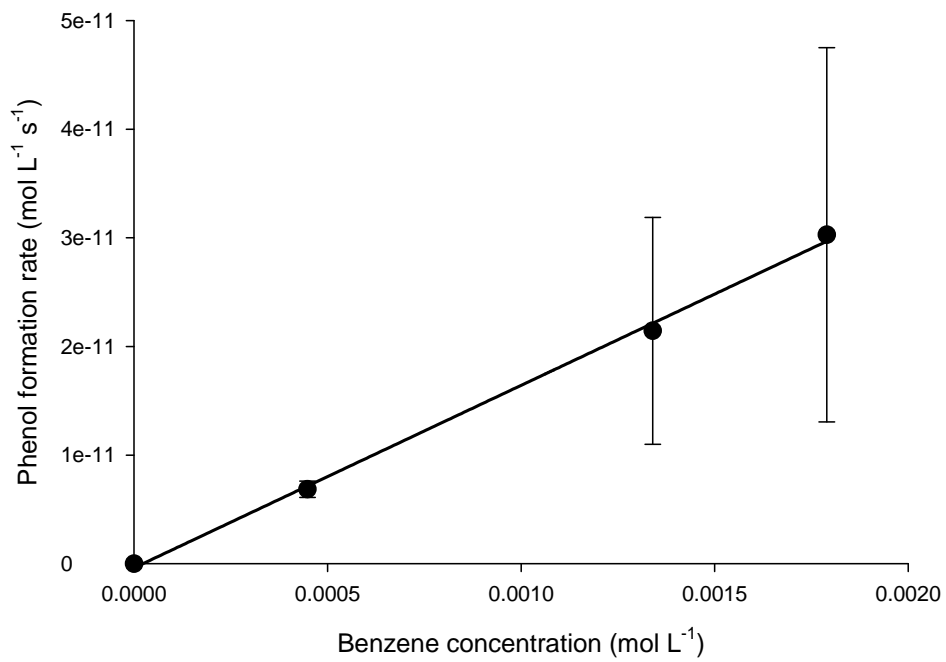(c

Light from Xe arc lamp

laser
radiation

Sample

Figure S1c

Figure S2

Figure S3

Figure S4